IRIS AperTO

UNIVERSITÀ DEGLI STUDI DI TORINO

AperTO - Archivio Istituzionale Open Access dell'Università di Torino

Shear zone liquefaction in mass transport deposit emplacement: A multi-scale integration of seismic reflection and outcrop data

This is the author's manuscript

Original Citation:

Availability:

This version is available http://hdl.handle.net/2318/149103 since

Published version:

DOI:10.1016/j.margeo.2014.05.001

Terms of use:

Open Access

Anyone can freely access the full text of works made available as "Open Access". Works made available under a Creative Commons license can be used according to the terms and conditions of said license. Use of all other works requires consent of the right holder (author or publisher) if not exempted from copyright protection by the applicable law.

(Article begins on next page)

06 May 2024

UNIVERSITÀ DEGLI STUDI DI TORINO

This Accepted Author Manuscript (AAM) is copyrighted and published by Elsevier. It is posted here by agreement between Elsevier and the University of Turin. Changes resulting from the publishing process - such as editing, corrections, structural formatting, and other quality control mechanisms - may not be reflected in this version of the text. The definitive version of the text was subsequently published in *[Marine Geology*, v.356, 2014, 50-64, doi: 10.1080/00206814.2014.931260].

You may download, copy and otherwise use the AAM for non-commercial purposes provided that your license is limited by the following restrictions:

(1) You may use this AAM for non-commercial purposes only under the terms of the CC-BY-NC-ND license.

(2) The integrity of the work and identification of the author, copyright owner, and publisher must be preserved in any copy.

(3) You must attribute this AAM in the following format: Creative Commons BY-NC-ND license (http://creativecommons.org/licenses/by-nc-nd/4.0/deed.en), **http://ees.elsevier.com/margo/**

Marine geology 4/2014, http://dx.doi.org/10.1016/j.margeo.2014.05-001

Shear zone liquefaction in mass transport deposit emplacement: A multi-scale integration of seismic reflection and outcrop data

Ogata, K. [1,5], Mountjoy, J.J. [2], Pini, G.A. [3], Festa, A. [4] and Tinterri, R.[5]

[1] Department of Arctic Geology, University Centre in Svalbard, P.O. Box 156, 9171, Longyearbyen, Norway (kei.ogata@gmail.com)

[2] National Institute of Water and Atmospheric Research, Private Bag 14901, Wellington, New Zealand (joshu.mountjoy@niwa.co.nz)

[3] Università degli Studi di Trieste, Dipartimento di Matematica e Geoscienze, 34128 Trieste, Italy (gpini@units.it)

[4] Dipartimento di Scienze della Terra, Università di Torino, 10125 Torino, Italy (andrea.festa@unito.it)

[5] Dipartimento di Fisica e Scienze della Terra "Macedonio Melloni", Università degli Studi di Parma, Campus Universitario - Parco Area delle Scienze 157/A, I-43124 Parma, Italy (roberto.tinterri@unipr.it)

Abstract

We present the integrated outcrop-geophysical study of two mass transport complexes, the exhumed Specchio unit in the Northern Apennines of Italy and the Holocene Poverty unit in the Hikurangi margin of New Zealand. The combination of micro- to meso-scale structural, stratigraphic and sedimentologic analyses carried on continuous three-dimensional outcrops, with large-scale structural and morphologic data deriving from seismic/acoustic imaging of the present-day continental margins, allow important considerations on submarine landslide processes and mechanisms through the broader (up-scaled and down-scaled) understanding of the mass transport-related structural associations. We compare the discontinuous high-amplitude, reverse-polarity reflectors observed within the Poverty with the syn-sedimentary, ductile shear zones found within the Specchio mass transport complex. The seismic signature of such structures suggests localized fluid overpressure along detachment/thrust zones due to shearing and loading of undrained, water-saturated, fine-grained material, developed along with the slide mass movement. The outcrop expression of these structures is tentatively attributed to m- to tens of m-thick shear zones comprising large amounts of sedimentary matrix which separate and accommodate the differential movements of the internal slide components (e.g. slide blocks, olistoliths). The sedimentary matrix is an unsorted, lithologically mixed medium characterized by a scale-invariant "block-in-matrix" fabric (i.e. brecciated, mud-supported), that injects, sustain and surrounds discrete slide elements (from particles to blocks) and interpreted as a hyper-concentrated (liquefied/fluidized) suspension of water and scattered sediments developed in fluid overpressure

conditions. We highlight the fundamental role of shearing-related liquefaction as one of the main factors controlling slide mobility through the "lubrication" of the internal and basal friction forces. The analysis of such features can therefore provide important information for the characterization of mass transport deposits developed from potentially catastrophic, long run-out mass transport events, and consequently, to better understand their possible socio-economic impact in terms of tsunamigenic potential.

Keywords: exhumed mass transport complexes; sedimentary matrix; ductile shear zones; liquefaction; fluid overpressure

1. Introduction

The recent achievements in marine geology on seafloor and sub-seafloor mapping allow important consideration on recent to modern submarine landslides, giving general clues on their overall morphology and areal extent (Canals *et al*., 2004; Frey-Martinez *et al*., 2006; Gee *et al*., 2007; Bull *et al.*, 2009). One of the main challenges arising from these studies revolves around the characterization of the complex internal anatomy of such deposits, and thus, the correct understanding of the genetic mechanisms and processes, which is crucial for offshore hydrocarbon exploration, and geohazard assessment and mitigation (see Hampton *et al.*, 1996; Mosher *et al.*, 2009; Kawamura *et al.*, 2012).

Most of the internal structures of a slide body are developed at the meso-scale (meters to ten of meters), and therefore hardly recognizable through geophysical methods being well below the standard seismic resolution. Moreover, the high internal heterogeneities and the combined occurrence of materials with different

degrees of consolidation contribute to complicate the seismic signal, resulting in acoustic artifacts and transparent zones. On the other hand, at the outcrop scale, these internal structures can be observed and described in detail (Lucente and Pini, 2003; Callot *et al.*, 2008a; 200b; Ogata *et al.*, 2012a), and, depending on the quality and the continuity of the exposures, such analyses could be up-scaled to fit to the seismic field of observation. In this framework we believe that a systematic comparison with fossil mass transport deposits cropping out in orogenic belts (i.e. sedimentary mélanges) would strongly contribute in solving these problems (Festa *et al.*, 2010a, 2010b, 2012). Currently, apart from the general and useful review of the mass transport deposits' seismic-scale structures provided by Bull *et al.* (2009) and the preliminary (and generally conceptual) attempt of comparison between seismic and outcrop data recently proposed by Bull and Cartwright (2010), there is still a general lack of works using an integrated approach in the study of submarine landslides. This leads to a gap in the basic knowledge of the meso-scale internal processes and related structures, and their relationship with larger scale features.

We present an attempt to combine and integrate geophysical and outcrop data in order to establish a continuity of observation at different scales, crucial for the study of vertically- and laterally-extensive submarine landslide deposits. Whereas the standard subsurface and seafloor imagery technology provides the gross morphology, areal extension and internal organization of a mass transport deposit, often providing a complete picture of a mass transport complex, the highest resolution of multi-channel seismic reflection data required to image such features is ca. 5 m or coarser. On the other hand, outcrop studies allow multi-scale analyses (depending on the exposure conditions), providing resolution from the microscopic scale up to the cartographic scale (comparable with the geophysical scale). Through the study of

100 comparable onland and offshore analogues it is virtually possible to fill the mutual
101 gaps of the two different approaches, allowing the construction of a more
102 comprehensive and better-constrained framework.

103 The aim of this work is to address these issues providing a detailed integration
104 of structural data coming from geophysical and outcrop examples characterized by
105 comparable scales and depositional settings. We present a compilation of outcrop data
106 coming from the Specchio mass transport complex, belonging to the Eocene-
107 Oligocene intra-slope basin succession (*i.e.* Epiligurian Units) developed atop the
108 exhumed Ligurian accretionary wedge in the Northern Apennines in Italy (Ogata *et*
109 *al.*, 2012a, 2012b). These field-based observations are tentatively up-scaled and
110 compared to the Holocene Poverty mass transport complex of the Hikurangi margin in
111 New Zealand (Mountjoy and Micallef, 2012).

112

113 **2. Geological background and case studies overview**

114 Our data come from two examples of large submarine mass failures emplaced in
115 subduction/collision-related wedge top depositional settings and characterized by
116 comparable physiographic and depositional contexts. The Specchio mass transport
117 complex is an ancient, exhumed example from the Northern Apennines of Italy, while
118 the Poverty mass transport complex comprises Holocene slide deposits emplaced in
119 an active subduction system off the East Coast of New Zealand (fig. 1). These two
120 examples are well suited for comparison as they are of a similar scale (both in terms
121 of areal extension and thickness), depositional setting (i.e. intra-slope, wedge-top) and
122 overall internal architecture (i.e. stacking/amalgamation of more events). These
123 general common features are summarized in the table of fig. 1C.

124

2.1 The Specchio mass transport complex

The upper Priabonian-lower Rupelian Ranzano Unit of the Epiligurian succession of the Northern Apennines represents a perfect example of syn-orogenic, siliciclastic infilling of an intra-slope, wedge-top mini-basin (i.e. small-scale) system characterized by depocenters about 5-10 km in size. These structurally confined basins were located atop the deforming Ligurian oceanic accretionary prism during its tectonic transport toward the eastern sectors, following the complex continental convergence between African (Adria) and European plates, in a time interval comprised between the latest stages of the Alpine orogenesis and the inflection (i.e. flexural down-bending) of the Apenninic foreland (Castellarin, 1994; Mutti *et al.*, 1995; Martelli *et al.*, 1998; Cavazza *et al.*, 2004; Marroni *et al.*, 2010).

The analyzed Specchio unit is a mass transport complex hosted in the middle-basal part of the Ranzano Sandstone stratigraphic succession (Martelli *et al.* 1998), which is mainly constituted by proximal, coarse-grained, low efficiency (*sensu* Mutti, 1992) turbidite deposits accumulated in relatively deep water setting (middle-upper bathyal depth; Di Giulio et al., 2002). This mass transport complex is characterized by an estimated areal extent conservatively calculated around ~ 1.500 km^2 and an average thickness of ~ 100 m, and it is generated by the rapid, polyphased accumulation of at least three mass transport deposits characterized by different paleo-transport directions: 1) a basal one(s), coming from the southern sectors, of mixed extra- and intrabasinal composition, originated from shallow-tectonic positive structures (e.g. anticline culminations) and other topographic highs close to the depocentral areas, 2) a middle one, coming from the northern sectors, of mainly intrabasinal composition, originated from structural highs located in a relatively distal position from the main depocenters, and 3) an upper one(s) coming from northern

150 sectors, composed of shallow-water related sediments failed from the basin margins,
151 in proximal position with respect to the inferred feeding areas (*i.e.* coastal areas) (fig.
152 2). In this framework, the Specchio unit is thought to represent the rapid sedimentary
153 response to a general rearrangement of the source-depositional system, operated by
154 the synergic effect of an active syn-sedimentary tectonism and sea level changes,
155 possibly acting together from the Early Oligocene (Ogata *et al.*, 2012b).

156 In terms of sedimentary processes, each individual depositional event comprises
157 a bipartite flow made up by a lower matrix-dominated and an upper block-dominated
158 parts (Ogata *et al.*, 2012a; 2012b) which in turn correspond to debris flows and blocky
159 flows, respectively (in the sense of Mutti *et al.*, 2006). The local occurrence of slump-
160 type deformations (i.e. coherent slide movement achieved through syn-sedimentary
161 shear zones; see Ogata *et al.*, 2012a) is restricted to the sand-dominated substrate and
162 the internally folded oversized blocks. The matrix composition and amalgamation,
163 and the various expressions of post-emplacement fluid escape and depressurization
164 acting together, suggest that the Specchio mass transport deposits are composed by (i)
165 a cohesive upper part (i.e. block-dominated portion), behaving as a relatively coherent
166 sheet of separated, passively-transported rafts ("rigid plug" of Middleton and
167 Hampton, 1973), and (ii) a non-cohesive, lower part (i.e. matrix-dominated portion)
168 behaving as a non-Newtonian fluid (hyperconcentrated suspension in the sense of
169 Mutti, 1992). In this framework, the matrix itself is thought to support internal slide
170 elements (from mm-sized clasts to m-sized blocks) due to its yield strength, whereas
171 at larger scale, the matrix-dominated portion is inferred to sustain the entire flow
172 through the upward and dispersive forces of the fluid excess pressure, reducing the
173 basal/internal frictions and enhancing the slide mobility (Ogata *et al.*, 2012a; 2012b;
174 Pini *et al.*, 2012). The same mechanisms have been also hypothesized for some

175 modern, long run-out submarine landslides (Mulder and Alexander, 2001).

176

177 **2.2 The Poverty mass transport complex**

178 The modern mass transport complex discussed in this paper occurs on the upper
179 slope of the Hikurangi Margin, an active subduction margin off the East Coast of New
180 Zealand (fig. 3) (Barnes *et al.*, 2010; Lewis and Pettinga, 1993).

181 The Poverty mass transport complex, also referred to as the Poverty Debris
182 Avalanche in literature, is the result of slope modification within the Poverty re-
183 entrant (Mountjoy and Micallef, 2012). The Poverty re-entrant is a margin-scale
184 morpho-tectonic feature interpreted to be the result of seamount impacts from the
185 incoming Pacific Plate, initiating approximately 1 Ma ago (Pedley *et al.*, 2010). The
186 structural and sedimentary post-impact reconfiguration of the margin is achieved by
187 the development of submarine canyon and slope-gully systems, as well as large-scale
188 mass failures (Orpin, 2004; Walsh *et al.*, 2007; Mountjoy *et al.*, 2009; Pedley *et al.*,
189 2010). In this area, Quaternary sedimentation developed thick shelf-basin sequences
190 and shelf-edge clinoforms, unconformably overlying, with draping and onlapping
191 relationships, Cretaceous to Miocene rocks, which are exposed in the gullies and
192 canyon heads of the Poverty re-entrant headwall (Mountjoy and Barnes, 2011).

193 The Poverty mass transport complex is one of the largest (~250 km^2) blocky
194 debris deposits of the Hikurangi margin, and covers most of the gently inclined (ca.
195 1°) seafloor of the Paritu basin between 1100 and 1500 m water depth. The deposit is
196 sourced from a restricted head area (34-46 km^3) below the shelf break (900-1150 m
197 water depth) and has likely failed in multiple (2-4), retrogressive depositional events
198 (Mountjoy and Micallef, 2012; Pouderoux *et al.*, 2012). Seismic reflection data
199 indicate complex internal deformation that is the topic of this study.

200

201 **3. Methods and data**

202 **3.1 The Specchio mass transport complex**

203 The Specchio mass transport complex has been primarily investigated through a
204 detailed field mapping (1:5.000 scale) to detail the overall internal and external
205 characteristics of the component mass transport deposits, their vertical and lateral
206 changes, relationships with the host sedimentary succession and general tectonic-
207 stratigraphic context.

208 High-resolution analyses and observations have been performed within the
209 different unit at various locations and stratigraphic levels in order to identify the
210 different mass transport facies (Ogata, 2012a; 2012b): meso- to micro-scale structural
211 and sedimentologic analyses have been performed to represent the spatial/geometric
212 distribution of the internal elements, their provenance and to highlight their bulk
213 deformation mechanism. Detailed stratigraphic logging (1:50 scale) of the over- and
214 underlying bedded successions has been performed to constrain the position of the
215 investigated unit within the sedimentary column and reconstruct the syn- to post-
216 depositional physiographic variations related to the slide emplacement.
217 Complementary micro-structural and sedimentologic analyses (i.e. transmitted light
218 optical microscopy) have been performed on thin sections coming from the
219 sedimentary matrix of the component mass transport deposits.

220 To clarify the used terminology, we here define as “ductile-like” the structures
221 showing mesoscale to microscale continuous deformation caused by independent (i.e.
222 intergranular) particulate flow occurred without appreciable mechanical grain
223 breakage (cataclasis, Knipe, 1986) within non-consolidated sediments with the
224 effective stress strongly reduced by fluid overpressure (mesoscopic ductile behavior;

225 Pini, 1999). By analogy, these structures (sometimes resembling metamorphic ductile
226 zones of concentrated deformation, such as the classical mylonites), are classified
227 with the standard terms (Passchier and Trouw, 2005) with the addiction of the suffix
228 "pseudo-" to stress their non-tectonic origin and the absence of any kind of intra-
229 crystalline plasticity, and used as kinematic indicators to solve the shearing sense of
230 the associated structures.

231 Since the identification of the source areas and the run-out paths is not obvious
232 in outcrop studies, we used a combination of the standard methods proposed in the
233 literature to unravel the local and general paleo-transport directions (Bradley and
234 Hanson, 1998; Lucente and Pini, 2003; Strachan and Alsop, 2006), collecting and
235 analyzing standard meso-structural data on plastic, soft-sediment deformation
236 structures and structural associations such as 1) non-cylindrical and asymmetrical
237 folds (i.e. vergences, axes, axial planes, plunges, sheath-fold main axes, etc.), and 2)
238 low-angle syn-sedimentary faults and shear zones (i.e. shear planes, lineations, long
239 axes of elongated elements, axes of associated drag folds, etc.), observed within the
240 matrix- and block-dominated parts of the component mass transport deposits bodies.
241

242 **3.2 The Poverty mass transport complex**

243 The Poverty mass transport complex has been imaged with a combination of
244 multibeam bathymetric data and multi-channel seismic reflection data. Multibeam
245 data on the continental slope are gridded at 25 m and are from Simrad EM300 and
246 EM302 surveys carried out between 2001 and 2011 (Mountjoy and Micallef, 2012;
247 Pedley *et al.*, 2010). Shelf/upper slope data, gridded at 10 m, include Simrad EM
248 3000 and Atlas Hydrosweep MD-2/30 (Royal New Zealand Navy) data. High-
249 resolution data are augmented with a regional 100 m bathymetric grid built from a

combination of 12 kHz SIMRAD EM12 Dual multibeam and single beam echo sounder bathymetric data held in the NIWA database. Three multichannel seismic reflection (MCS) datasets are presented in this study: 1) 6-fold, 24-channel seismic profiles acquired with a GI-gun source in 45/105 mode in 2001, 2) up to 960-channel high fold 2D seismic reflection data recorded to 12 seconds TWT in 2005, and 3) 12-fold, 48-channel seismic profiles acquired with a twin GI-gun source in 45/105 mode in 2011 (Barker *et al.*, 2009; Mountjoy and Barnes, 2011; Pedley *et al.*, 2010). An assumed sediment velocity of 1.800 m/s has been used for volume calculations and time-depth conversion.

4. Results

4.1. The Specchio mass transport complex

Ductile-like, syn-sedimentary shear-zones are commonly expressed by low-angle thrust and subordinately normal faults, sometimes and locally steep-dipping, affecting both matrix and blocks but with different characteristics. Such shear zones are represented by discrete intervals, centimeters- to several meters-thick and meters- to tens of meters-long, characterized by a contrasting texture with the surrounding lithologies. These structures do not show discrete shear surfaces or planes, being instead represented by intervals of remolded and mixed appearance, due to the internal occurrence of elongated bands and lenses of sedimentary matrix, comprising different types of pseudo-ductile shearing clues: 1) pseudo-SC (i.e. Shear/Cleavage) structures, 2) pseudo-Sigma structures, 3) hydroplastic, intrafolial folds, 4) iso-orientation of rigid oblate clasts, 5) preferential elongation of plastic intra-clasts, 6) disaggregation/deformation bands and 7) rheomorphic-like, fluidal structures (fig. 4).

Depending on the composition and consolidation degree of the involved

materials, these shear zones are usually characterized by a local enhancement in the concentration of matrix, developed through frictional deformation and disaggregation of the involved sediments. The internally banded pattern, defined by isoclinally folded and elongated mud intraclasts and particle alignments, is generally coherent with the associated shear plane testifying shearing in overall visco-plastic conditions (fig. 5).

The basal shear zone is usually thicker and more laterally continuous than the internal ones and it is also typically characterized by the occurrence of higher amount of intrabasinal, liquefied material belonging to the substrate. Secondary internal shear zones mainly develop along the boundaries of discrete slide elements (*i.e.* blocks, un-dissociated masses), comprising a relatively small amount of matrix arranged in discontinuous pinching-and swelling seams and lenses. Sometimes such shear zones are rooted into the basal shear interval, suggesting that the same liquefied material of the basal shear zone has been injected upward (fig. 6).

Microstructural observations performed on thin sections reveal no evidence of tectonic-related brittle deformations (*e.g.* cataclasis, syn-kinematic mineralized veins or fractures, stylolites) within such structures. Microinjections of matrix into preexisting discontinuities and voids affecting the single grains (0.5 mm scale), pseudo deformation/disaggregation bands, iso-orientation of elongated particles and fluidal structures suggest shearing under low confining stress and generalized fluid overpressure conditions (fig. 7). These observations are supported by the results of experimental and numerical modeling, as summarized in Goren *et al.*, (2010) and Goren *et al.* (2011).

Combining the structural data from the shear zones, tuned with the above-mentioned kinematic indicators used to define the general shearing sense, with the spatial distribution of asymmetric folds (i.e. separation-arc, mean-axis and sheath-fold

300 long axis methods; Bradley and Hanson, 1998; Lucente and Pini, 2003; Alsop and
301 Holdsworth, 2004; Strachan and Alsop, 2006), and the arrangement of the internal
302 element imbrication (Ogata *et al.*, 2012a, 2012b), an overall down-slope transport
303 direction has been estimated for each component mass transport deposits. The general
304 vergence and the stacking relationships of these shear zones, mostly represented by
305 low-angle thrusts arranged in splays and imbricated sets, provide additional kinematic
306 information to understand their mechanism and mode of emplacement.

307 Structural associations typically align parallel to the inferred position of the
308 lateral boundaries of the slide mass (i.e. slide margins/levees). Detailed observations
309 on three-dimensional outcrops, integrated with the estimation of paleo-transport
310 directions, highlight a strong lateral anisotropy/heterogeneity of the internal meso-
311 scale structural arrangement, either in cross and longitudinal view. In cross section
312 (i.e. looking parallel to the slide movement), this is evident from the common
313 occurrence of low-angle shear zones and structural associations (e.g. pop up- and
314 flower structures, double-vergent box folds, sheath folds, folds' interference patterns)
315 characterized by non-concordant to opposite shearing and verging sense recording an
316 overall lateral buckling transversally to the mean transport direction, whereas in long
317 section (i.e. looking laterally to the slide movement) they appear to record an overall
318 preferential down-slope direction (fig. 8).

319

320 **4.2 The Poverty mass transport complex**

321 The internal structure of the Poverty mass transport complex is revealed in
322 multi-channel seismic reflection data (MCS). Mass transport deposits are identified by
323 discontinuous weak reflectivity compared to the overall coherent reflectivity of the
324 host sediments (e.g. Lamarche *et al.*, 2008).

In multibeam data the upper surface of the Poverty mass transport complex is irregular and it shows a blocky roughness characterized by marked lateral changes. The uneven surface of the deposit is given by the presence of individual rafted slide blocks varying from ca. 1000 m across in the up-slope part to less than 100-150 m in the down-slope part, defining two different portions of the slide mass characterized by different geometry and roughness characteristics (figs. 3C). In cross section, these slide blocks appear as localized zones with internally coherent and continuous reflectors, sometimes deformed but usually pseudo-concordant with the basal surface, surrounded by a background of discontinuous reflectors and transparent zones (see figs. 3D and 9E).

Down with the length of the landslide body we recognize distinctive longitudinal transformations in the structural style. Within the upper portion of the body, thrusts and folds, indicating a compressional regime, dominate the structural style. Further down the length of the slide mass, structures become more subdued and dominated by normal faulting, indicating down-slope tensions within the debris body. These structures show curved to roughly rectilinear axes, mostly disposed perpendicular to the inferred slide movement and becoming progressively parallel to it toward the slide margins, following the overall lobate-like shape of the slide body.

In the down-slope portion, the deposit indicates compressional deformation in multiple locations, as suggested by the occurrence of tens of meters-sized thrust faults defined by hanging wall and footwall cutoffs. In places it is apparent that internal units have been thrust over one another (figs. 9B and 9C).

Remarkably, the above described thrust faults are in many cases accompanied by high amplitude reflectors bounding the surface that define the basal *décollement*. These internal discontinuous reflectors are commonly defined by inverse polarity,

350 indicating discrete low-density contrast zones (figs. 9D and 9E). As recognized
351 elsewhere in seismic reflection data (e.g. Bull *et al.*, 2009; Yamada *et al.*, 2012) the
352 basal slide horizon is a distinct unit of lower acoustic impedance compared to the
353 coherent high amplitude underlying reflectors below (defining non-mass transport
354 sedimentation), which may be extensively deformed or completely scoured by the
355 overlying material (Vardy *et al.*, 2012). Accordingly, the semi-continuous, coherent
356 reflectors found within the slide body are interpreted to separate (at least 2) different
357 deposits from the same general source area (see figs. 9D and 9E).
358
359 **5. Discussion**
360 **5.1 Mass transport-related liquefaction/fluidization: processes and products**
361 Within the analyzed slide masses liquefaction/fluidization-related structures
362 generally develop above a main, basal shear zone and, depending on the mechanical
363 coupling between sliding mass and substrate, also into the underlying succession.
364 Evidence of liquefaction/fluidization processes is the sedimentary matrix
365 represented by an unsorted, hyper-concentrated mixture of loose and poorly
366 consolidated fine-grained sediments. This element is a fundamental component of a
367 slide body along with other discrete parts that behave coherently (*e.g.* slide blocks,
368 un-dissociated masses, *etc.*), usually marking the internal and basal shear zones as
369 discontinuous or continuous, cm- to m-sized (and up to tens of m-sized) elongated
370 lenses and bands, respectively.
371 Our data suggest that the basic deformation mechanism is the high-rated,
372 generalized shearing of undrained (i.e. water saturated, low-permeability) sediments
373 at low confining stress and fluid overpressure conditions. Besides the herein proposed
374 process, instantaneous frictional heating is another possible mechanism able to cause

increase pore pressure up to liquefaction (Goren and Aharonov, 2007).

As observed from both outcrop and geophysical data, most of the shearing achieved during the slide movement is likely accommodated within the basal interval, resulting in a sort of "overpressured carpet" that mechanically separates the slide mass from the substrate due to hampered hydraulic diffusivity. These overpressured basal interval are represented in a mass transport deposits by the lower matrix-dominated portions on outcrop and by the high-amplitude, inverse polarity reflectors on seismic profiles.

When the mechanical coupling becomes strong enough (*e.g.* during slide mass deceleration and freezing), the momentum can then be partly transferred downward, with the consequent involvement of the underlying sediments. This deformation is likely caused by dynamic/static overloading and rear push of the sliding mass. A similar geophysical evidence of this kind of mass transport-induced substrate deformation and incorporation (i.e. erosion in sedimentological meaning) is for instance shown by the high-resolution seismic profiles of small-scale lacustrine mass transport deposits provided by Schnellmann *et al.* (2005).

At the scale of the entire slide mass, compressional stress is mainly located at the front of the slide mass and then, transferred to the surrounding sediments. Folding and thrusting at various scales are the most common structural evidence of these processes in outcrops. The external arrangement of the final mass transport deposit is therefore characterized by low- to high-angle thrusts, isolated and/or rooted in the basal shear plane (*i.e.* blind thrusting), forming meso- to mega-scale folds which culminations may deform the upper surface forming elongated topographic highs (*e.g.* "pressure ridges"). At this scale, these shear zones seem to develop some kind of "backstepping" trend, following the upslope migration of the deformation kink-point

400 due to the progressive stopping of slide mass front and margins.

401 During the emplacement, the extensional structures achieved during the failure
402 and transport phases are thus likely overprinted and/or reworked in a generally
403 compressive regime, as suggested by the predominance of compressional features
404 recorded in the outcrop database.

405

406 **5.2 Post-depositional processes and consequences**

407 It is important to note that post-depositional processes seem to play a major role
408 in the final anatomy of a slide body, as observed on ancient (Strachan, 2002, 2008)
409 modern examples (Diviacco *et al.,* 2006; Moernaut *et al.*, 2009; Rebesco *et al.*, 2009;)
410 and inferred from experimental and numerical modeling (Major and Iverson, 1999;
411 Major, 2000). During the early post-depositional compaction, the internal fluid
412 overpressure may be dissipated through developing of fluid-escape structures,
413 sometimes reaching the slide surface as mud/sand volcanoes, or can be retained for a
414 relatively long time interval, favoring slow differential movements of the entire mass.
415 Such later movements develop as a generalized creeping of the upper surface of the
416 slide deposit, with decreasing displacement towards its bottom, reworking and
417 crosscutting earlier stage structures.

418 If the boundary conditions are favorable (*e.g.* slope steepness, weak layers in the
419 substrate prone to liquefy, *etc.*) the frontal impact of a slide mass against seafloor
420 highs or preceding landslide accumulations, and secondary movements of the deposit
421 during the post-depositional stage may reactivate the material accumulated at the front
422 of the body causing another secondary slide to start ("progressive landsliding"). This
423 is well expressed in the frontal part of the Poverty mass transport complex, where the
424 impact of secondary events has had a significant impact on the surface morphology

425 and the internal structure of the landslide complex. Towards the upper portion of the
426 slide, where extensional deformation may be expected repeated blocky failures
427 impacting the upper slide debris have formed a zone dominated by large scale
428 compressional deformation and thrust faulting. Towards the distal end of the
429 landslide, where compression may be expected and particularly in frontally confined
430 landslides, the landslide body shows widespread extension related to remobilization
431 of the debris interpreted to occur in response to compressional impacts in the upper
432 slide mass (fig. 10b). Further complicating this framework, smaller, secondary slide
433 events, mainly in form of flows, may occur on the upper surface of slide masses,
434 during the transport, accumulation and post-depositional stages.
435
436 **5.3 Conceptual model of the internal mass transport deposit deformation**
437 Combining the observations made on the two investigated mass transport
438 deposits we tentatively propose a conceptual model of the deformation mechanisms
439 acting within the slide mass, from up-slope to down-slope, on the basis of the amount
440 of sedimentary matrix and its dominant position within the deposit. This model is
441 represented in fig. 11.
442 In this framework the bulk of the deformation (both within the slide mass and in
443 the underlying substrate) and the consequent *loci* of enhanced matrix production is
444 supposed to be located where the slope gradient of the basal shear interval changes
445 (e.g. flat-ramp transition, slope-basin transition, intra-basinal or intra-slope seafloor
446 morphology).
447 It is important to point out that the described slide masses evolve within a
448 morphologically confined setting. The resulting internal deformation and related
449 structures are thus strongly influenced by the forced frontal and lateral

compression/transpression with the intrabasinal highs, slide levees and the other preceding slide deposits. In a relatively unconfined depositional context, such as a foredeep basin plain, the frontal part of the slide mass could instead virtually spread out over long distances with the resulting development of mainly extensional/transtensional structures at the top of the slide masses (Lucente and Pini, 2003). Similar characteristics have been also observed in the morpho-bathymetric and seismic profiles of Eastern Mediterranean Slope, where frontally-confined and frontally-emergent mass transport complexes have been described (Frey-Martinez *et al.*, 2006).

Further work is planned to include in the model the lateral variations in the deformation style of the slide anatomy due to structural confinement.

6. Conclusions

Seismic reflection data reveal large-scale characteristics of emplacement processes in a complete mass transport complex, whereas outcrop analyses provide subtle details of controlling failure processes. The integration of the two different approaches is crucial for the correct understanding of the submarine landslide dynamics. Our key results are summarized as follows:

1) Liquefaction, fluidization and soft-sediment deformation are common processes in the internal structural evolution of submarine landslide bodies. The final product of such processes is an overpressured sedimentary matrix localized within discrete shear zones, which accommodate internal and basal friction forces, eventually enhancing slide mobility.

2) The main mechanisms invoked are a combination of (i) undrained shearing of water-saturated, poorly-consolidated sediments due to dragging forces acting along internal elements' boundaries (internal differential movements) and at the very base of the slide mass (down-slope movement), and (ii) dynamic loading and un-loading cycles due to the pulsating nature of the mass transport events.

3) At the scale of the entire deposit, such zones of concentrated fluid excess pore pressure can be visualized in seismic profiles, especially at the very base of the unit where horizons of trapped high fluid pressure may induce high amplitude reflectivity and even negative polarity. Such reflectors can be observed also within the slide mass, and depending on their lateral continuity, may indicate the amalgamation surface/interval between two subsequent bodies, therefore representing a powerful tool to distinguish single depositional units (mass transport deposits) from composite, multiple accumulation complexes (mass transport complexes).

4) The whole slide mass can be longitudinally subdivided into different zones characterized by different stress regime and consequent deformation mechanisms, as evidenced by the different relative amount of sedimentary matrix.

The systematic integration of available geophysical data with detailed outcrop studies represents the most reliable method for the study of submarine landslides. This synergic approach permits observations covering all the scales (from the microscopic to the regional scale) and allows overcoming the intrinsic resolution limits of the single methods. Accordingly, the hypotheses coming from the modern marine

499 geology surveys can be tested and calibrated directly on selected analogues on the
500 field, and *vice versa*, especially in terms of genetic and evolutionary processes and
501 slide dynamics, which in turn represent the key factors that control forecasting and
502 mitigation of submarine landslide-related geohazards.
503
504 **Acknowledgments**
505 We would like to thank Hans-Juergen Gawlick, Dusan Plasienka and an
506 anonymous reviewer for having deeply improved the quality of the manuscript with
507 their constructive comments and suggestions. Joshu Mountjoy supported by NIWA
508 under Coasts and Oceans Research Programme 1 (2013/14 SCI).
509
510 **References**
511
512 Alsop, G.I., Holdsworth, R.E. 2004. The geometry and topology of natural sheath
513 folds: a new tool for structural analysis - Journal of Structural Geology, v. 26,
514 1561–1589.
515 Barker, D.H.N., Sutherland, R., Henrys, S., Bannister, S., 2009. Geometry of the
516 Hikurangi subduction thrust and upper plate, North Island, New Zealand.
517 Geochem. Geophys. Geosyst., 10.
518 Barnes, P.M., Lamarche, G., Bialas, J., Henrys, S., Pecher, I.A., Netzeband, G.L.,
519 Greinert, J., Mountjoy, J.J., Pedley, K., Crutchley, G., 2010. Tectonic and
520 Geological Framework for Gas hydrates and Cold Seeps on the Hikurangi
521 Subduction Margin, New Zealand. Marine Geology 272(1-4), 26-48.
522 Bradley, D., Hanson, L., 1998. Paleoslope Analysis of Slump Folds in the Devonian
523 Flysch of Maine. Journal of Geology 106, 305–318.

524 Bull, S., Cartwright, J., 2010. Small-Scale Insights into Seismic-Scale Slumps: A
525 Comparison of Slump Features from the Waitemata Basin, New Zealand, and
526 the Møre Basin, Off-Shore Norway. In D.C. Mosher *et al.* (Eds.), Submarine
527 Mass Movements and Their Consequences, 257 Advances in Natural and
528 Technological Hazards Research 28, 257-266.
529 Bull, S., Cartwright, J., Huuse, M., 2009. A review of kinematic indicators from
530 mass-transport complexes using 3D seismic data. Marine and Petroleum
531 Geology 26/7, 1132-1151.
532 Callot, P., Odonne, F., Sempere, T., 2008a. Liquification and soft-sediment
533 deformation in a limestone megabreccia: The Ayabacas giant collapse,
534 Cretaceous, southern Peru. Sedimentary Geology 212, 49–69.
535 Callot, P., Sempere, T., Odonne, F., Robert, E., 2008b. Giant submarine collapse of a
536 carbonate platform at the Turonian-Coniacian transition: The Ayabacas
537 Formation, southern Peru. Basin Research 20, 333–357. doi: 10.1111/j.1365-
538 2117.2008.00358.x.
539 Canals, M., Lastras, G., Urgeles, R., Casamor, J.L., Mienert, J., Cattaneo, A., De
540 Batist, M., Haflidason, H., Imbo, Y., Laberg, J.S., Locat, J., Long, D., Longva,
541 O., Masson, D.G., Sultan, N., Trincardi, F., Bryn, P., 2004. Slope failure
542 dynamics and impacts from seafloor and shallow sub-seafloor geophysical
543 data: case studies from the COSTA project. Marine Geology 213, 9-72.
544 Castellarin, A., 1994. Strutturazione eo-mesoalpina dell'Appennino Settentrionale
545 attorno al "nodo ligure. In: Capozzi, R., Castellarin, A. (Eds.), Studi
546 preliminari all'acquisizione dati del profilo CROP 1–1A La Spezia–Alpi
547 orientali. Studi Geologici Camerti, Volume Speciale 1992/2: Camerino,
548 Università degli Studi di camerino, 99-108.

549 Cavazza, W., Roure, F., Ziegler, P.A., 2004. The Mediterranean area and the
550 surrounding regions: active processes, remnants of former Tethyan oceans and
551 related thrust belts. In: Cavazza, W., Roure, F., Spakman, W., Stampfli, G.M.,
552 Ziegler, P.A. (Eds.), The TRANSMED Atlas: The Mediterranean Region from
553 crust to mantle. Springer, 1–29.
554 Di Giulio, A., Mancin, N., Martelli, L., 2002. Geohistory of the Ligurian orogenic
555 wedge: first inferences from Epiligurian sediments. Boll. Soc. Geol. It., Spec.
556 vol. 1, 375-384.
557 Diviacco, P., Rebesco, M., Camerlenghi, A., 2006. Late Pliocene mega debris flow
558 deposit and related fluid escapes identified on the Antarctic Peninsula
559 continental margin by seismic reflection data analysis. Marine Geophysical
560 Research 27, 109–128.
561 Festa, A., Dilek, Y., Pini, G.A., Codegone, G., Ogata, K., 2012. Mechanisms and
562 processes of stratal disruption and mixing in the development of mélanges and
563 broken formations: Redefining and classifying mélanges. Tectonophysics 568-
564 569, 7-24, doi: 10.1016/j.tecto.2012.05.021.
565 Festa, A., Pini, G.A., Dilek, Y., Codegone, G., 2010a. Mélanges and mélange-forming
566 processes: a historical overview and new concepts, in: Dilek, Y. (Ed.), Alpine
567 Concept in Geology. Int. Geol. Rev. 52 (10-12), 1040-1105, doi:
568 10.1080/00206810903557704.
569 Festa, A., Pini, G.A., Dilek, Y., Codegone, G., Vezzani, L., Ghisetti, F., Lucente,
570 C.C., Ogata, K., 2010b. Peri-Adriatic mélanges and their evolution in the
571 Tethyan realm, in: Dilek, Y. (Ed.), Eastern Mediterranean geodynamics (Part
572 II). Int. Geol. Rev. 52 (4-6), 369-406, doi: 10.1080/00206810902949886.

573 Frey-Martinez, J., Cartwright, J., James, D., 2006. Frontally confined versus frontally
574 emergent submarine landslides: a 3D seismic characterization. Marine and
575 Petroleum Geology 23, 585-604.
576 Gee, M.J.R., Uy, H.S., Warren, J., Morley, C.K., Lambiase, J.J., 2007. The Brunei
577 slide: A giant submarine landslide on the North West Borneo Margin revealed
578 by 3D seismic data. Marine Geology 246/1, 9-23.
579 Goren, L., Aharonov, E. 2007. Long run-out landslides: the role of frictional heating
580 and hydraulic diffusivity. Geophysical Research Letters 34, 1-7.
581 Goren, L., Aharonov, E., Sparks, D., Toussaint, R. 2010. Pore pressure evolution in
582 deforming granular material: A general formulation and the infinitely stiff
583 approximation, J. Geophys. Res. 115, B09216.
584 Goren, L., Aharonov, E., Sparks, D., Toussaint, R. 2011. The Mechanical Coupling of
585 Fluid-Filled Granular Material Under Shear. Pure and Applied Geophysics
586 168, 10.1007/s00024-011-0320-4.
587 Hampton, M.A., Lee, H.J., Locat, J., 1996. Submarine Landslides. Rev Geophys 34,
588 33-59.
589 Kawamura, K., Sasaki, T., Kanamatsu, Y., Arito, S., Ogawa, Y., 2012. Large
590 submarine landslides in the Japan Trench: A new scenario for additional
591 tsunami generation. Geophys Res Lett 39, L05308
592 Knipe, R.J., 1986. Deformation mechanism path diagrams for sedi- ments undergoing
593 lithification. In: Moore, J. C. (Ed.), Structural Fabrics in D. S. D. P. Cores
594 from Forearcs. Mem. geol. Soc. Am. 166, 151-160.
595 Lamarche, G., Joanne, C., Collot, J.-Y., 2008. Repetitive Large Submarine Mass
596 Transport Complexes in the South-Kermadec Forearc Basin: The Matakaoa

Submarine Instability System. Geochemistry Geophysics Geosystems 9(4), Q04001.

Lewis, K.B., Pettinga, J.R., 1993. The emerging, imbricate frontal wedge of the Hikurangi margin. In: Ballance P.F. (Ed.), South Pacific sedimentary basin. Sedimentary Basins of the World 2. Elsevier Sciences publishers, Amsterdam, pp. 225-250.

Lucente, C.C., Pini, G.A. 2003. Anatomy and emplacement mechanism of a large submarine slide within a Miocene foredeep in the Northern Appennines, Italy: a field perspective. American Journal of Science 303, 565-602.

Macdonald, D.I.M, Moncrieff, A.C.M., Butterworth, P.J., 1993. Giant slide deposits from a Mesozoic fore-arc basin, Alexander Island, Antarctica. Geology 21/11, 1047-1050.

Major, J.J., 2000. Gravity-driven consolidation of granular slurries: implications for debris-flow deposition and deposit characteristics. Journal of Sedimentary Research 70/1, 64-83.

Major, J.J., Iverson, R.M., 1999. Debris-flow deposition: effects of pore-fluid pressure and friction concentrated at flow margins. GSA Bulletin 111, 1424–1434.

Marroni, M., Meneghini, F., Pandolfi, L., 2010. Anatomy of the Ligure-Piemontese subduction system: evidence from Late Cretaceous–middle Eocene convergent margin deposits in the Northern Apennines, Italy. Int. Geol. Rev. 52, 1160-1192.

Martelli, L., Cibin, U., Di Giulio, A., Catanzariti, R., 1998. Litostratigrafia della Formazione di Ranzano (Priaboniano sup.-Rupeliano, Appennino Settentrionale e Bacino Terziario Ligure Piemontese). Boll. Soc. Geol. It., vol. 117, 151-185.

622 Middleton, G.V., Hampton, M.A., 1973. Sediment gravity flows: mechanics of flow
623 and deposition. - In. Middleton G.V., Bouma, A.H. (Eds.), Turbidites and
624 Deep-water Sedimentation. SEPM Pacific Section, Short Course Notes, 1-38.
625 Moernaut, J., De Batist, M., Heirman, K., Van Daele, M., Pino, M., Brümmer, R.,
626 Urrutia, R., 2009. Fluidization of buried mass-wasting deposits in lake
627 sediments and its relevance for paleoseismology: results from a reflection
628 seismic study of lakes Villarrica and Calafquén (South-Central Chile).
629 Sedimentary Geology 213, 121–135.
630 Mosher, D.C., Austin, J.A. Jr., Fisher, D., Gulick, S.P.S., 2009. Deformation of the
631 northern Sumatra accretionary prism from high-resolution seismic reflection
632 profiles and ROV observations. Marine Geology 252, 89–99.
633 Mountjoy, J., Barnes, P., Pettinga, J., 2009. Morphostructure of submarine canyons on
634 an active margin: Cook Strait Canyon system, New Zealand. Marine Geology
635 260, 45–68. doi:10.1016/j.margeo.2009.01.006.
636 Mountjoy, J.J., Barnes, P.M., 2011. Active upper-plate thrust faulting in regions of
637 low plate-interface coupling, repeated slow slip events, and coastal uplift:
638 Example from the Hikurangi Margin, New Zealand. Geochem. Geophys.
639 Geosyst., 12, Q01005. doi:10.1029/2010GC003326.
640 Mountjoy, J.J., Micallef, A., 2012. Polyphase Emplacement of a 30 km3 Blocky
641 Debris Avalanche and Its Role in Slope-Gully Development. In: Y. Yamada,
642 K. Kawamura, K. Ikehara, Y. Ogawa, R. Urgeles, D. Mosher, J. Chaytor, M.
643 Strasser (Eds.), Submarine Mass Movements and Their Consequences.
644 Advances in Natural and Technological Hazards Research. Springer,
645 Netherlands, pp. 213-222.

646 Mulder, T., Alexander, J., 2001. The physical character of subaqueous sedimentary
647 density flows and their deposits. Sedimentology 48, 269-299.
648 Mutti, E., Carminatti, M., Moreira, J.L.P., Grassi, A.A., 2006. Chaotic Deposits:
649 examples from the Brazilian offshore and from outcrop studies in the Spanish
650 Pyrenees and Northern Apennines, Italy. A.A.P.G. Annual Meeting, April 9-
651 12, Houston, Texas.
652 Mutti, E., Papani, L., Di Biase, D., Davoli, G., Mora, S., Segadelli, S., Tinterri, R.,
653 1995. Il Bacino Terziario Epimesoalpino e le sue implicazioni sui rapporti tra
654 Alpi ed Appennino. Memorie di Scienze Geologiche di Padova 47, 217 – 244.
655 Mutti, E.,1992. Turbidite Sandstones. San Donato Milanese, Agip-Istituto di
656 Geologia, Università di Parma, 275 pp.
657 Ogata, K., Mutti, E., Pini G.A., Tinterri, R., 2012a. Mass transport-related stratal
658 disruption within sedimentary mélanges. Tectonophysics 568-569, 185-199.
659 Ogata, K., Tinterri, R., Pini, G.A., Mutti, E., 2012b. The Specchio Unit (Northern
660 Apennines, Italy): an ancient mass transport complex originated from near-
661 coastal areas in an intra-slope setting. In: Yamada, Y., Kawamura, K., Ikehara,
662 K., Ogawa, Y., Urgeles, R., Mosher, D., Chaytor, J., Strasser, M. (Eds.),
663 Submarine Mass Movements and Their Consequences. Advances in Natural
664 and Technological Hazards Research. Springer Netherlands, 595-605.
665 Orpin, A.R., 2004. Holocene sediment deposition on the Poverty-slope margin by the
666 muddy Waipaoa River, East Coast New Zealand. Marine Geology 209, 69-90.
667 Passchier, C.W., Trouw, R.A., 2005. Microtectonics. Springer Berlin Heidelberg New
668 York, 365 pp.
669 Pedley, K.L., Barnes, P.M., Pettinga, J.R., Lewis, K.B., 2010. Seafloor structural
670 geomorphic evolution of the accretionary frontal wedge in response to

671 seamount subduction, Poverty Indentation, New Zealand. Marine Geology
672 270(1-4), 119-138.
673 Pini, G.A., Ogata, K., Camerlenghi, A., Festa, A., Lucente, C.C., Codegone, G., 2012.
674 Sedimentary mélanges and fossil mass-transport complexes: a key for better
675 under- standing submarine mass movements? In: Yamada, Y., Kawamura, K.,
676 Ikehara, K., Ogawa, Y., Urgeles, R., Mosher, D., Chaytor, J., Strasser, M.
677 (Eds.), Submarine Mass Movements and Their Consequences. Advances in
678 Natural and Technological Hazards Research. Springer Netherlands, 585-594.
679 Pini, G.A.,1999. Tectonosomes and olistostromes in the Argille Scagliose of the
680 Northern Apennines, Italy. Geol. Soc. of America Special 335, 73 pp..
681 Pouderoux, H., Lamarche, G., Proust, J.N., 2012. Building an 18 000-year-long paleo-
682 earthquake record from detailed deep-sea turbidite characterisation in Poverty
683 Bay, New Zealand. Nat Hazard Earth Sys, 12(6), 2077-2101.
684 Rebesco, M., Neagu, R.C., Cuppari, A., Muto, F., Accettella, D., Dominici, R., Cova,
685 A., Romano, C., Caburlotto, A., 2009. Morphobathymetric analysis and
686 evidence of submarine mass movements in the western Gulf of Taranto
687 (Calabria margin, Ionian Sea). Int. J. Earth Sci. (Geol. Rundsch.) 98, 791–805.
688 DOI 10.1007/s00531-009-0429-1
689 Schnellmann, M., Anselmetti, F. Giardini, D., McKenzie, J. 2005. Mass movement-
690 induced fold-and-thrust belt structures in unconsolidated sediments in Lake
691 Lucerne (Switzerland). Sedimentology 52, 271–289. doi: 10.1111/j.1365-
692 3091.2004.00694.x
693 Strachan, L.J., 2002. Slump-initiated and controlled syndepositional sandstone
694 remobilization: an example from the Namurian of County Clare, Ireland.
695 Sedimentology 49, 25-41.

696 Strachan, L.J., 2008. Flow transformations in slumps: a case study from the
697 Waitemata Basin, New Zealand. Sedimentology 55, 1311–1332.
698 Strachan, L.J., Alsop, G.I., 2006. Slump folds as estimators of palaeoslope: a case
699 study from the Fisherstreet Slump of County Clare, Ireland. Basin Research
700 18, 451-470.
701 Vardy, M.E., L'Heureux, J.-S., Vanneste, M., Longva, O., Steiner, A., Forsberg, C.F.,
702 Haflidason, H., Brendryen, J. 2012. Multidisciplinary investigation of a
703 shallow near–shore landslide, Finneidfjord, Norway. Near Surface Geophysics
704 10(4), 267-277. (doi:10.3997/1873-2012022).
705 Walsh, J.P., Alexander, C.R., Gerber, T., Orpin, A.R., Sumners, B.W., 2007. Demise
706 of a submarine canyon? Evidence for highstand infilling on the Waipaoa River
707 continental margin, New Zealand. Geophysical Research Letters 34, L20606.
708 Woodcock, N.H., 1979. The use of slump structures as palaeoslope orientation
709 estimators. Sedimentology 26/1, 83 – 99.
710 Yamada, Y., Kawamura, K., Ikehara, K., Ogawa, Y., Urgeles, R., Mosher, D.,
711 Chaytor, J., Strasser, M. (Eds.), 2012. Submarine Mass Movements and Their
712 Consequences. Advances in Natural and Technological Hazards Research,
713 Springer Netherlands.
714
715 **Figure caption**

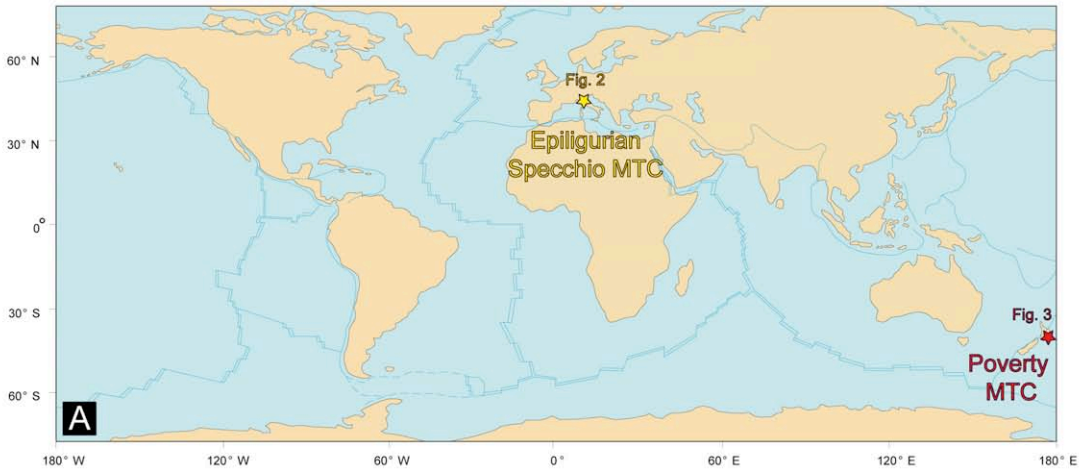

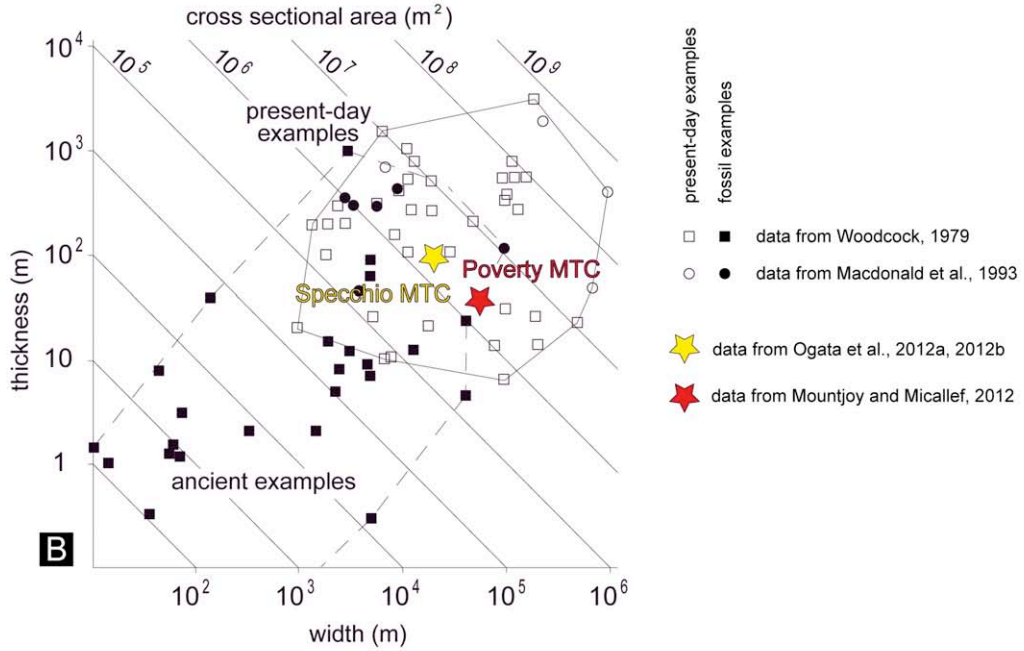

Average component MTDs	Length (km)	Width (km)	Area (km2)	Volume (km3)	Depth range (m)	Max. thickness (m)	Component MTDs (Nr.)	Slide element max. cross-sectional length (m)	Internal characteristics	External morphology	Depositional Setting	Source area	Reference
Specchio MTC	45*	20*	380*	75*	500-2000*	300	≥ 3	up to 200	Bipartite deposit with a slump-like, block-dominated upper part and a debris flow-like, matrix-dominated lower part	Uneven upper surface draped by turbidite-type deposits and strongly erosive basal surface. High lateral thickness variability and amalgamations.	Intra-slope, wedge top, confined basin system	shelf-shelf edge-upper slope	Ogata, 2010
Poverty MTC	35	15	250	33.5	1100-1500	250	≥ 2	up to 500-1000	Weak, semi continuous coherent reflectors separated by transparent to faintly reflective zones	Irregular blocky upper surface roughness with longitudinal variations, with larger blocks in the upslope part and smaller blocks in the downslope part. Strongly erosive basal surface. High lateral thickness variations.	Intra-slope, wedge-top, confined fore-arc basin	upper slope	Mountjoy and Micallef, 2012

C

*based on extrapolation of field observations

716

717 Figure 1: A) Geographic location of the two case studies. B) Thickness vs. width
718 diagram showing relative sizes of ancient (dashed line envelope) and present-
719 day (solid line envelope) mass transport deposits (MTDs) and mass transport
720 complexes (MTCs). The relative dimensions o the two studied examples are

plotted. Modified from Lucente and Pini (2003) after Woodcock (1979) and Macdonald et al. (1993). C) Table listing the parameters of comparison between the two analyzed examples: the Specchio MTC (Italy) and the Poverty MTC (New Zealand).

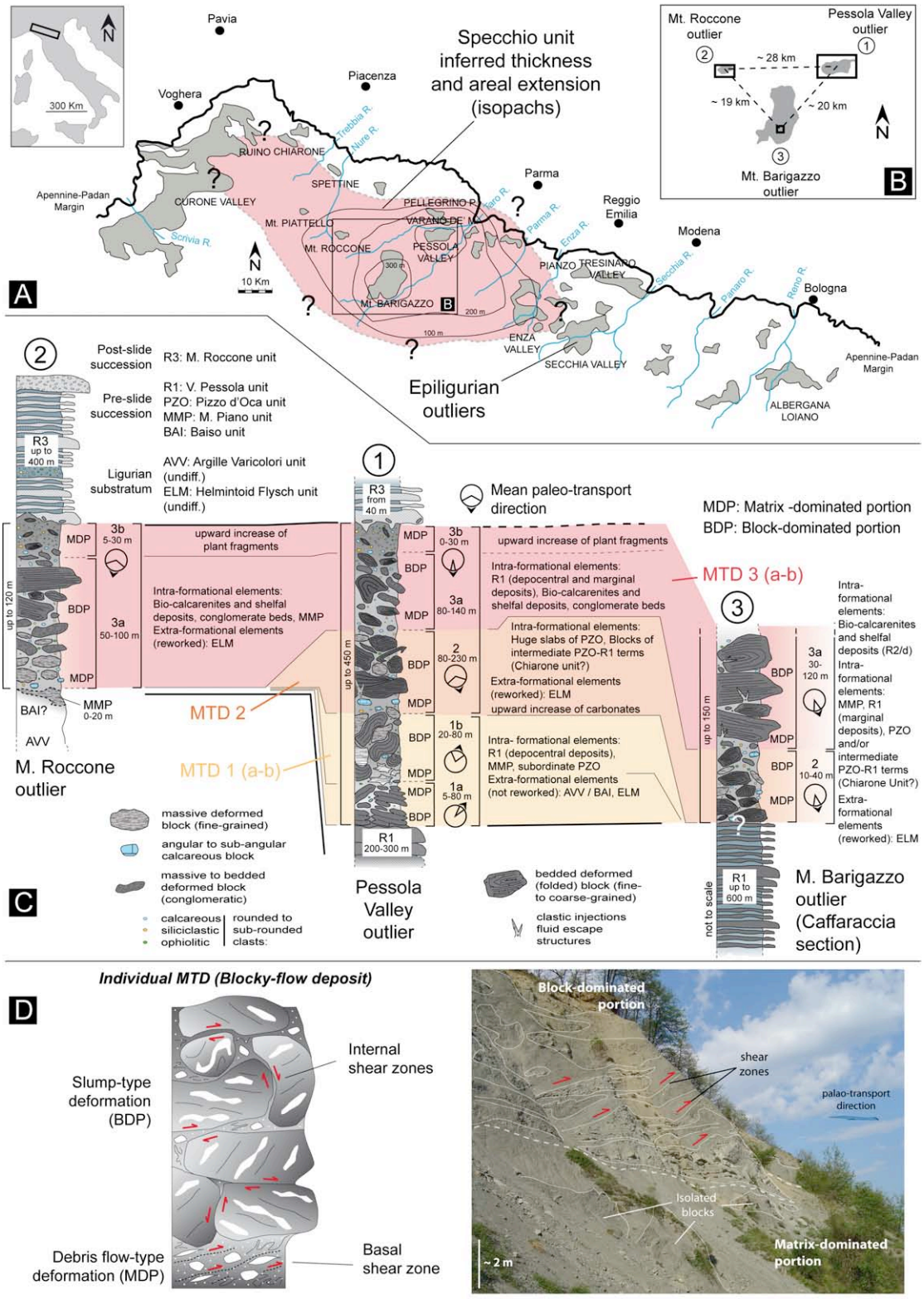

Figure 2: A) Schematic representation of the sedimentary remnants (i.e. outliers) of the Epiligurian succession scattered across the eastern side of the Northern Apennines (location in the left inset). Redrawn and modified from Martelli et

al. (1998). B) Close up of A showing the reciprocal distances and location of the three Epiligurian outliers (i.e. Pessola Valley, Mt. Roccone and Mt. Barigazzo sections) where the Specchio MTC has been investigated. C) Simplified stratigraphic logs and correlation of the Specchio MTC across the three investigated Epiligurian outliers (location in B). The internal subdivisions, lithologies, main component and mean paleo-transport directions are labeled (modified after Ogata et al., 2012a, 2012b). D) Schematic log of a blocky flow deposits, showing the basic component MTD of the Specchio unit. In the photograph a line drawing of the MTD 2 (see C) labeling the main structural elements is depicted.

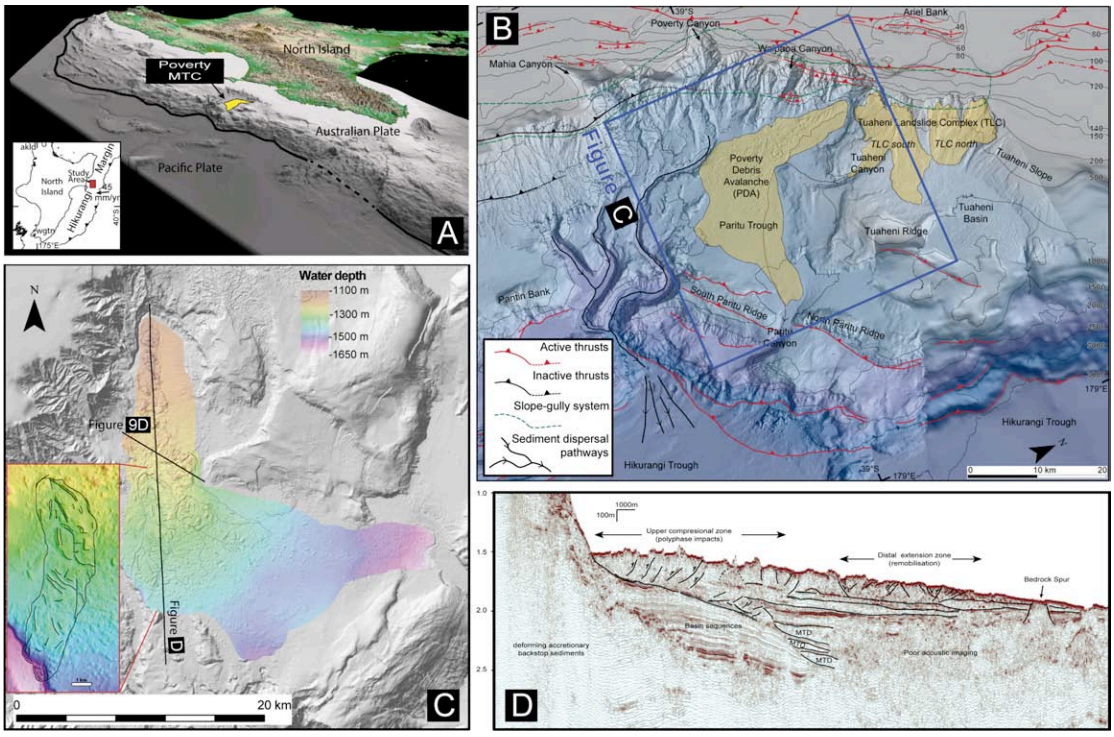

Figure 3: A) Bird's eye view of the northeastern continental margin of New Zealand (looking toward the SW; location of the area in the inset). Plate boundaries and position of the investigated Poverty MTC are labeled. B) Interpreted geomorphic map of the upper Poverty Re-entrant showing the main MTDs (labeled in yellow) and the major characterizing structures (see explanation

inset). C) Morphologic map of the Poverty MTC with water-depth ranges indicated. The inset shows a secondary superficial failure (i.e. subordinate MTD) affecting the frontal part of the main MTD. MCS profiles' paths shown in D and Fig. 9D are labeled. D) Internal stratigraphy of the Poverty MTC and host sedimentary succession as resolvable in MCS data. The entire length of the Poverty MTC is covered, showing in particular 1) an upslope compressional part and a downslope extensional part (labeled) due to base-of-slope accumulation, 2) a complex basal flat-ramp erosional surface (basal solid line) and 3) weak, discontinuous internal reflectors suggesting the amalgamation of at least 2 main depositional events (internal solid lines). In addiction, the underlying sedimentary succession is characterized by the occurrence of at least 3 other MTDs testifying that submarine landsliding is a recurrent process in this setting.

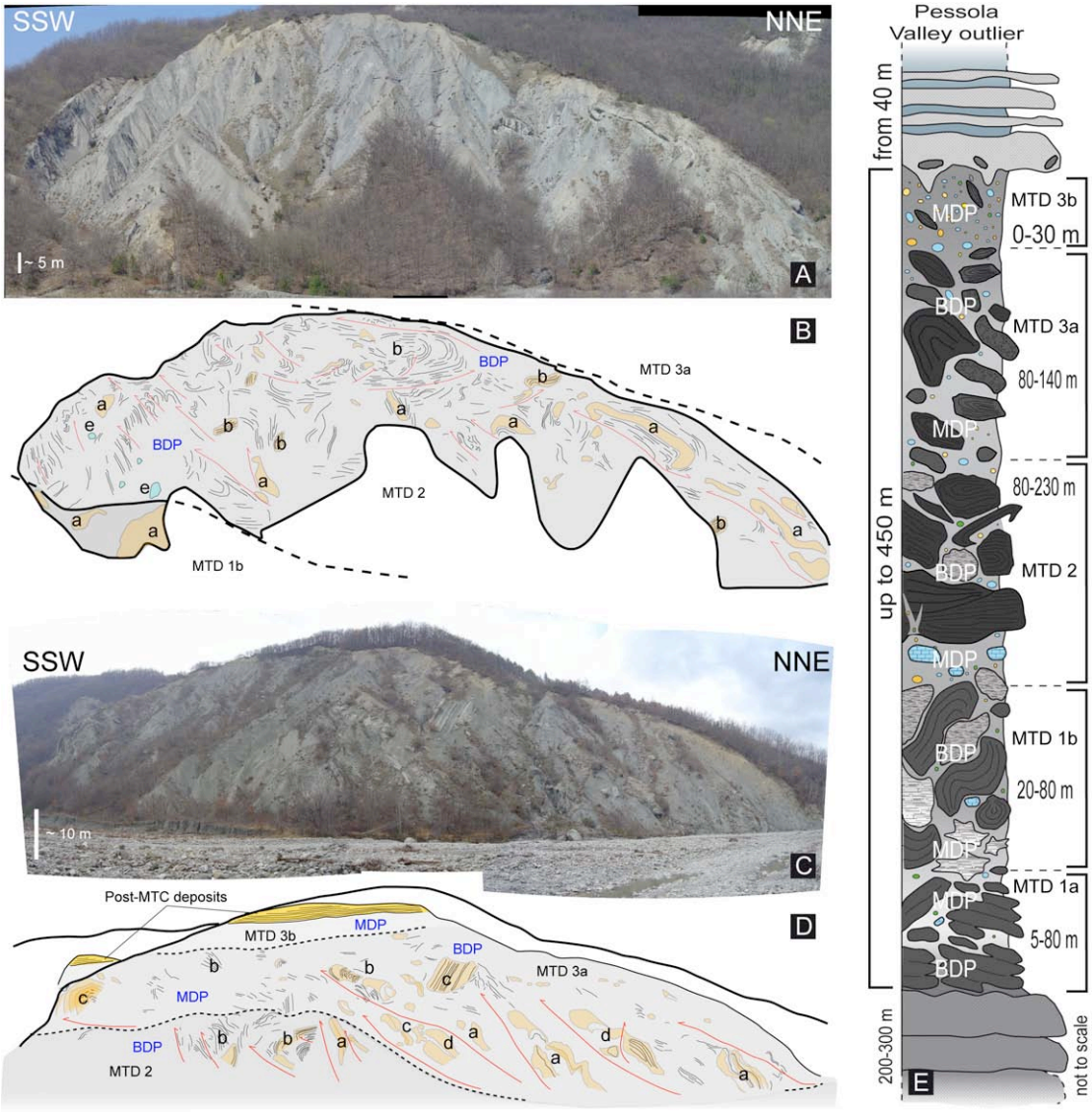

758

759 Figure 4: Early Rupelian Specchio MTC (Pessola Valley section). A) Photomosaic of
760 the middle component (MTD 2) of the Specchio unit. B) Interpretation and
761 line drawing of the recognizable internal bedding (black lines). C)
762 Photomosaic of the upper component (MTD 3) of the Specchio unit. D)
763 Interpretation and line drawing of the main structures. E) Simplified
764 stratigraphic column of the Specchio MTC in the type locality in the Pessola
765 Valley outlier. The component MTDs and the relative thickness ranges are
766 indicated. Explanation of labels in B and D: a - thick-bedded, coarse-grained
767 sandstone elements; b - thin-bedded, fine-grained sandstone-mudstone

elements; c - medium-bedded, fine- to medium-grained sandstone-siltstone elements; d - pebbly to cobbly conglomerate elements; e - carbonate elements; MDP - matrix-dominated portion; BDP - block-dominated portion.

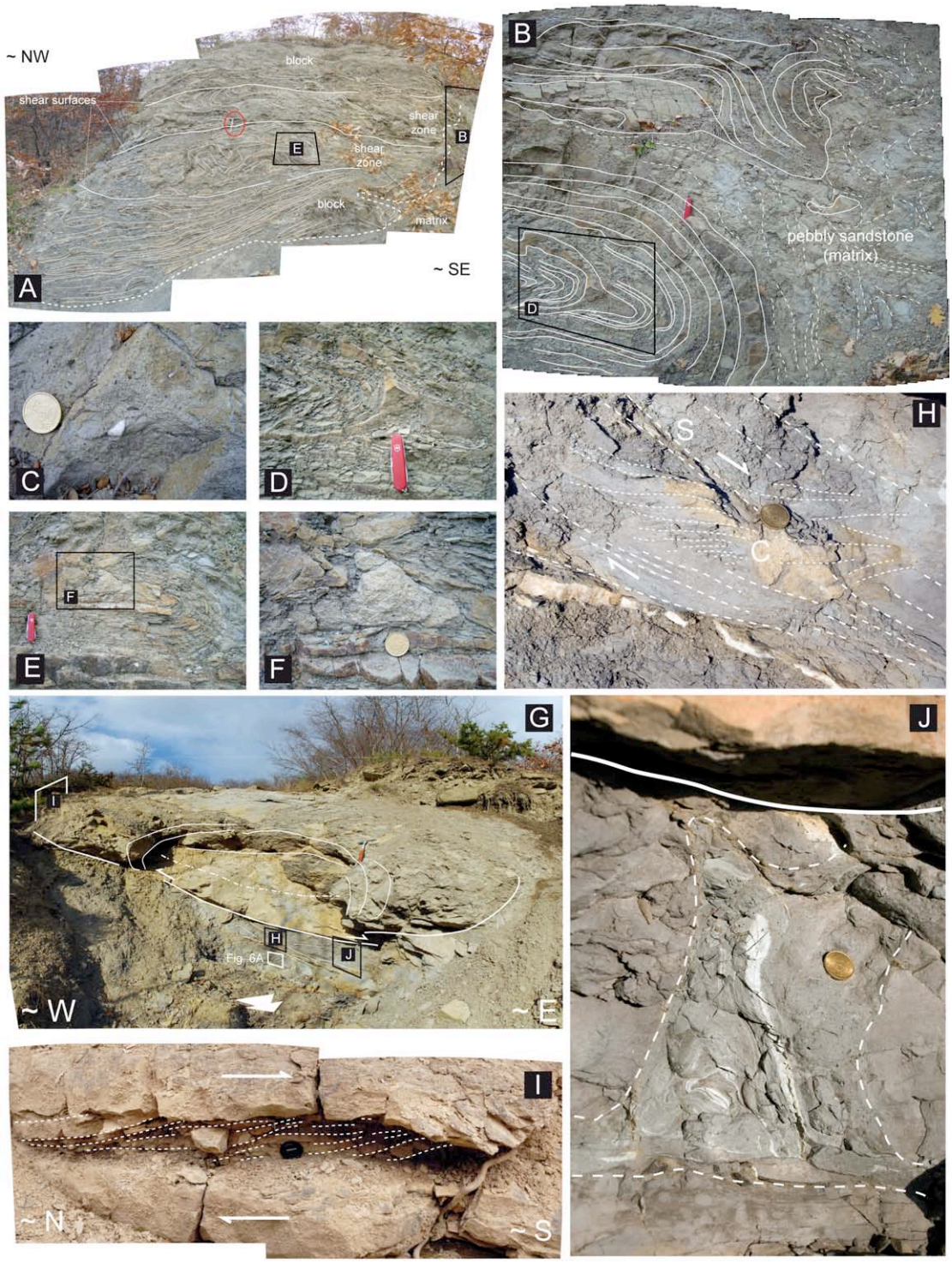

Figure 5: Early Rupelian Specchio MTC (Mt. Roccone section), MTD 2. A) Photomosaic and line drawing of ductile-like shear zones affecting a slide

774 block made up of thin-bedded sandstone-mudstone interlayers. Circled
775 hammer for scale. B) Close-up of A showing the soft sediment folds (solid
776 lines) and the fluidal structures within the host sedimentary matrix (dashed
777 lines) at the slide block lateral boundary (location in A). This matrix forms
778 sub-horizontal injection into the slide block roughly along the termination of
779 the shear planes labeled in A. C) Detail of the sedimentary matrix showing
780 well-rounded pebbles and granules dispersed within a fine-grained unsorted
781 sedimentary matrix containing well-rounded pebbles and granules dispersed
782 within a clayey-marly lithology. D) Close-up of the isoclinal fold represented
783 in B, showing the extreme, localized thickening of a cm-thick sandstone bed in
784 the hinge zone, testifying liquefaction of the sandy material. E) Close-up of A
785 showing an isoclinal synform fold with the upper limb truncated and matrix
786 injection along the axial plane. F) Detail of E showing the injected matrix into
787 the fold's hinge zone. G) A cm-thick shear zone (thick solid line and white
788 arrows indicating the shear sense) overlain by a slide block made of thin-
789 bedded, fine-gained sandstone layers (thin solid lines) plastically deformed
790 into a meso-scale sheath fold (axis trend marked by dashed line). The white
791 arrow indicates the mean paleo-transport direction inferred. H) Close-up of the
792 shear zone in G showing the ductile-like, pseudo-SC shear structures (dotted
793 lines). White arrows indicate the inferred shear sense. I) Detail of the shear
794 zone in G showing sigmoidal-type structures and small-scale duplexes (dotted
795 lines). The inferred shear sense is labeled (white arrows). J) Close up of the
796 base of the slide block in G showing upward matrix injections (e.g. fluid
797 escape) rooted in the shear zone. Note the fluidal structures defined by
798 extremely plastically deformed marly intraclasts within the pebbly mudstone.

799

800

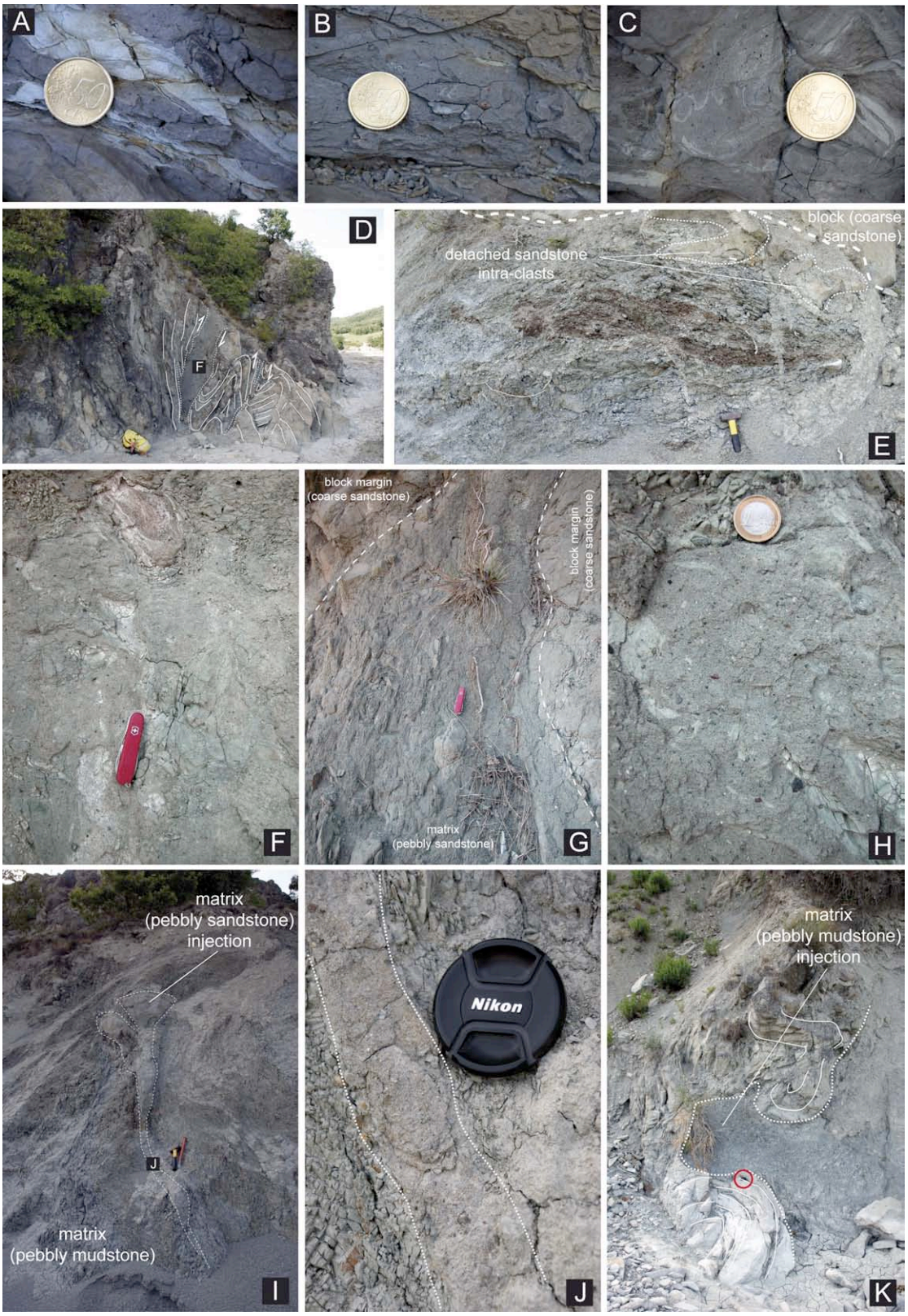
A
B
C
D
F
detached sandstone
intra-clasts
block (coarse
sandstone)
E
F
block margin
(coarse sandstone)
block margin
(coarse sandstone)
matrix
(pebbly sandstone)
G
H
matrix
(pebbly sandstone)
injection
J
matrix
(pebbly mudstone)
I
Nikon
J
matrix
(pebbly mudstone)
injection
K

801

802 Figure 6: Early Rupelian Specchio MTC (Pessola Valley and Mt. Roccone sections);
803 lower-middle MTDs 2 and 3. A) Example of sedimentary matrix coming from
804 a cm-thick shear zone (location in fig. 5G). Note the shearing-related,
805 asymmetric boudinage of the marly intraclasts. B) Example of the unsorted,
806 pebbly mudstone sedimentary matrix. Some elements, especially the elongated
807 intraclasts, show a rough iso-orientation of the long axes. C) Example of the
808 fluidal structures (e.g. hydroplastic folds) found within the sedimentary matrix
809 shown in B. D) Thick (ca. 60 cm) shear zone marked by a discontinuous band
810 of unsorted, mixed and generally massive pebbly sandstone in a sandy block-
811 dominated portion. E) A detached isoclinal fold developed in an exotic
812 (Cretaceous Ligurian AVV unit, see text) shaly slide block at the boundary
813 between the matrix- and block-dominated portions. F) Detail of the shear zone
814 in D showing the appearance of the pebbly sandstone matrix. Note the
815 hydroplastically folded, fine sandstone and mudstone intraclasts. G) Matrix-
816 rich shear zone developed at the lateral contact between two slide blocks
817 within the block-dominated portion shown in D. The pebbly sandstone matrix
818 displays pseudo-SC shears and rotated/deformed clasts characterized by
819 pseudo-sigma shapes. H) Detail of the host pebbly sandstone/mudstone matrix
820 characterizing the matrix-dominated portion. Note the overall alignment and
821 the iso-orientation of the mudstone intraclasts. I) Dome-topped pebbly
822 sandstone dyke injecting into the host pebbly mudstone matrix of the matrix-
823 dominated portion in E. This structure suggests later (i.e. post-depositional)
824 liquefaction of pressurized discrete sandy elements (i.e. slide blocks) with
825 consequent intrusion into the more impermeable, compacting host pebbly
826 mudstone matrix. J) Close up of I showing in detail the pebbly-sandy material

comprising the matrix injection. K) Dome-shaped lateral injection of host pebbly mudstone matrix into a sandstone block with associated plastic folding of the sandstone beds. Circled lens cap for scale.

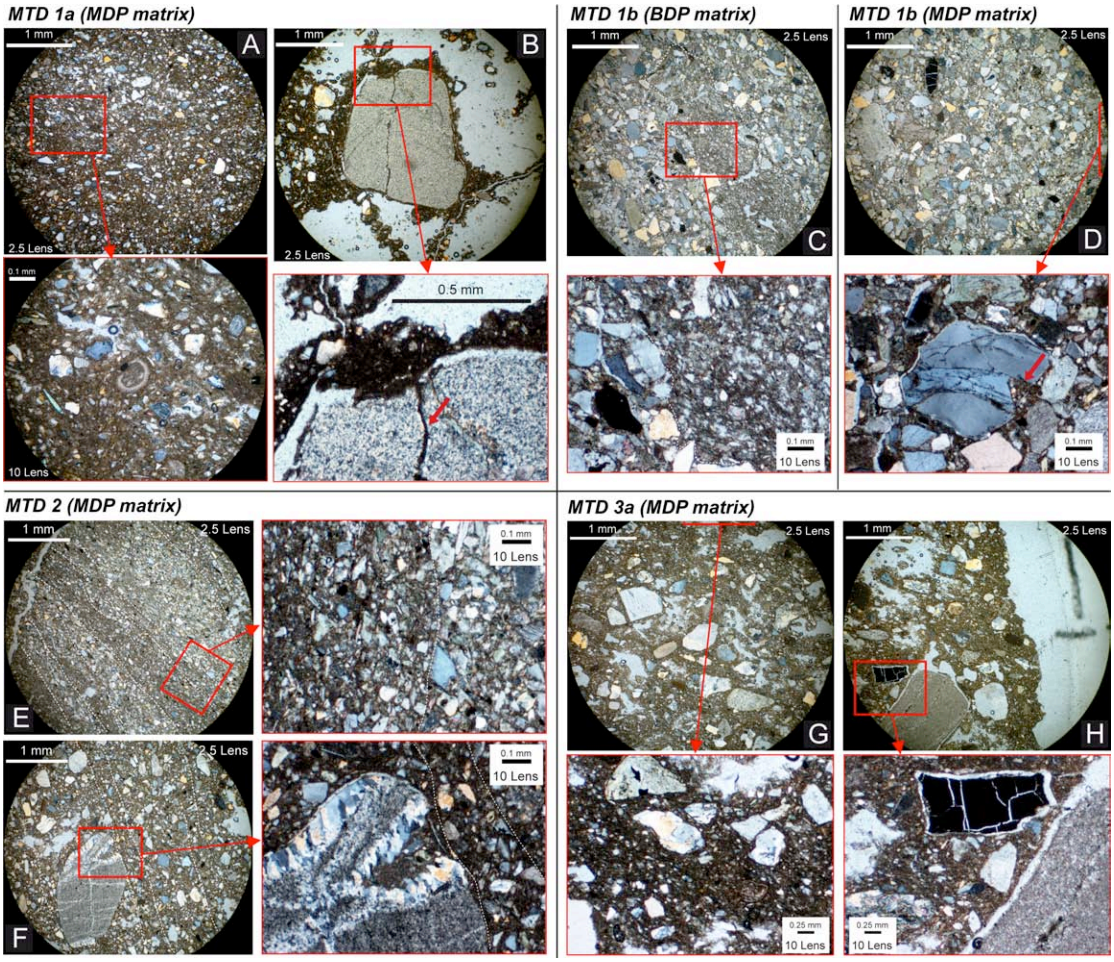

Figure 7: Early Rupelian Specchio MTC, optical microscope observations of the matrix for each component MTD. A) Fine-grained portions of the matrix showing the "brecciated" texture and the occurrence of both rounded and angular grains. Close-up: detail of the finer granulometric population of the matrix. Note the occurrence of well-preserved microfossils (radiolarians?) and the "fluidal" appearance of the finer matrix, enveloping grains and filling voids between elements. B) Sub-rounded lithic grain showing a fracture filled with finer material of the host matrix. Close-up: detail the injection of fine-grained matrix within the fracture (red arrow). This evidence indicates fluid

overpressure conditions of the matrix, possibly up to hydro-fracturing. C) Medium- to coarse-grained sand particles with mud infillings within inter-granular spaces. Elongated patches of fine-grained material, sharing the same characteristics of the muddy component are aligned to the overall oblique banding (from the upper-left to the lower-right), expressed by iso-orientation of grains' long axes and by elongated clustering of particles sharing similar dimensions. Close-up: detail of the transitional border of the fine-grained elongated patches with the surrounding matrix material. The fine-grained lithology is the same of that filling inter-granular spaces and sustaining sandy particles. Note the "fluidal" appearance of the fine-grained material and the development of faint planar discontinuity (e.g. psudo-foliation) marked by the preferential alignment of elongated/platy grains. D) Matrix with fine-grained material more diffused and diluted within the sandy grains, and lineations and banding less evident. The overall appearance is more "matrix-sustained" than that observed in C. Partial close up: detail of a fractured sub-angular quartz grain, characterized by a thin calcite halo, and surrounded by fine-grained material. The latter seems to inject into internal voids of the grain (red arrow); other minor injections along fractures are present. Along with this, the fine-grained material envelops particles (even where grains are almost in contact) testifying its plastic/fluidal nature. E) Matrix showing a thinly banded appearance. Note the fine-grained material arranged in "ribbon"-like patches. Lineations are also highlighted by the preferential alignment of particles, along their long axis. Close-up: boundary between two relatively fine- and coarse-grained elongated clusters. These structures suggest overall simple shear conditions achieved through an independent particulate flow without

cataclasis (i.e. grain breakage) and, are here defined as pseudo-deformation/disaggreagation bands. F) Homogeneous unsorted matrix. The well-rounded, mm-sized, lithic pebble (metamorphic?) observable in the lower-left side of the photo is internally characterized by the intrusion of the finer material into the voids left by leached out, previously mineralized vein. Note also the faintly recognizable shear-like band passing tangentially to the upper-right margin of largest pebble, and trending obliquely the photo, from the upper-left side to the lower-right side (boundaries labeled with white dashed lines). Close-up: detail of the primary mineralized vein and the injected fine-grained material. This evidence supports the fluid-like state of the matrix. Note the fluidal-like appearance of the surrounding matrix, simulating pebble boundaries. G) Rigid particles dispersed and sustained within a fine-grained, unconsolidated lithology. Partial close-up: relationships between particles and the finer material, which envelopes grains and seems to be structurally arranged in a crude oblique lineation (deformation bands-like structures), as underlined by particles alignment. H) Overview of the matrix close to a major, mm-sized, well-rounded pebble of sedimentary origin. Close-up: detail the finer matrix surrounding the pebble. Note the presence of a coal fragment (vegetal organic matter) enveloped by a thin calcite halo, as observed for the other rigid elements.

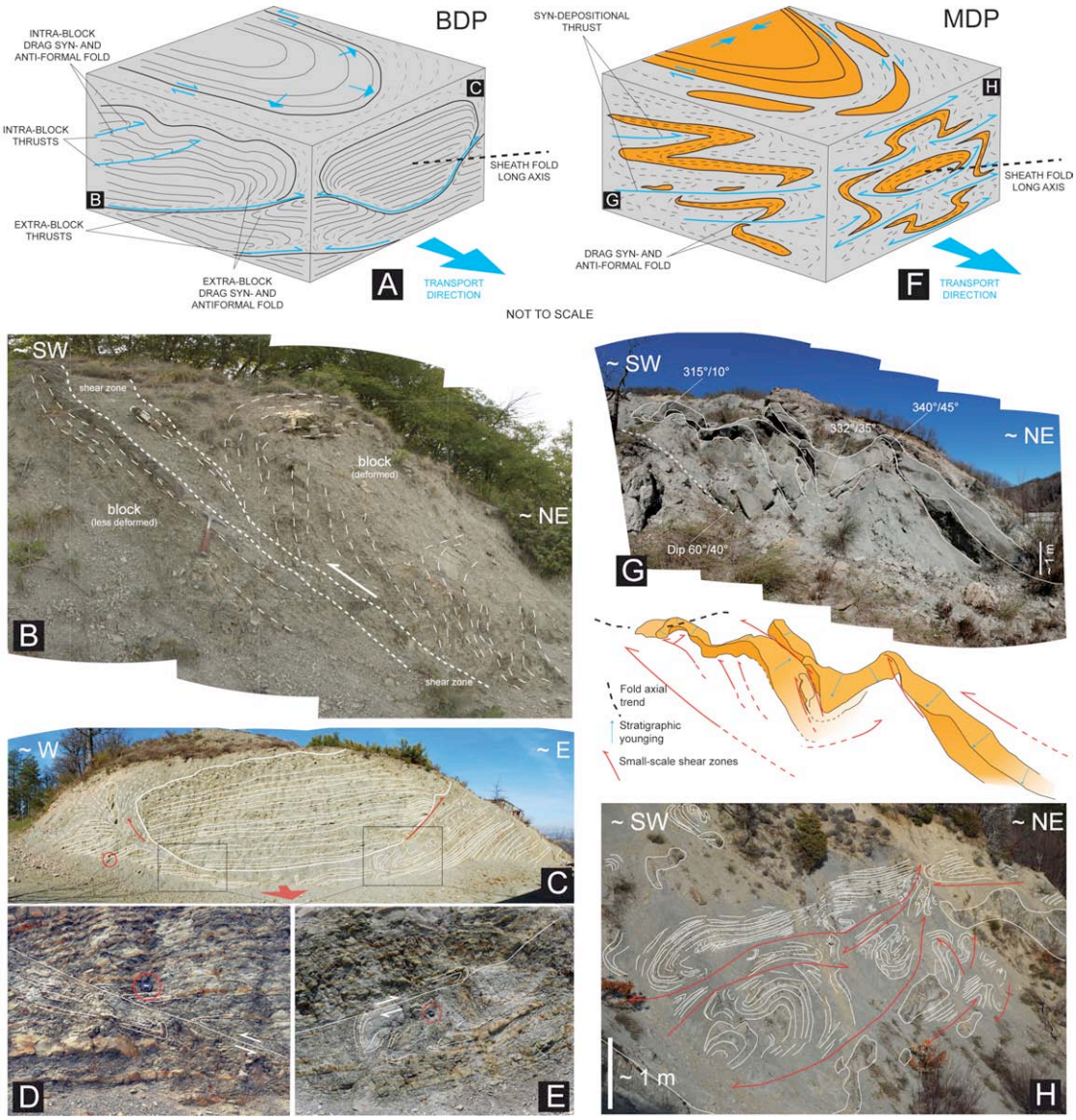

885

886 Figure 8: Early Rupelian Specchio MTC (Pessola Valley outlier). A) Conceptual
887 block diagram representing structural associations (inspired from Bradley and
888 Hanson, 1998), which characterize block-dominated portions (BDP).
889 Representative features and relative structural data used for kinematic analysis
890 are indicated. B) Photo-mosaic and line drawing representing a shear zone
891 underlined by a matrix horizon, which separates two block portions (intra-
892 block thrust). This structural association represents the longitudinal side of the
893 block diagram shown in A. Hammer for scale. C) Photo-mosaic and line
894 drawing showing a block overriding another through an intra-block shear

zone. The cut is roughly perpendicular to the main inferred transport direction (transparent red arrow). D) and E) Close-ups showing in detail the same shear surface characterized by two apparent opposite shear senses. This structural association represents the transversal side of the block diagram shown in A. Hammer and Camera lens cap (circled) for scale, 7 cm in diameter. F) Conceptual block diagram representing structural associations (inspired from Bradley and Hanson, 1998), which characterize matrix-dominated portions (MDP). Representative features and relative structural data used for kinematic analysis are indicated. G) Photo-mosaic and interpretation of a meso-scale folding system involving a single thick, coarse-grained sandstone bed, comprised within a MDP (structural data are labeled). Asymmetries and relative vergences are roughly uniform (apart from few minor backthrusts). Note the sheath-like geometry shown by the main fold apex (left side). This structural association represents the longitudinal side of the block diagram shown in F. H) Photo and line drawing of a MDP characterized by complex folding due to the occurrence of several opposite verging shear zones, causing a generalized buckling of structures. This structural association represents the transversal side of the block diagram shown in F.

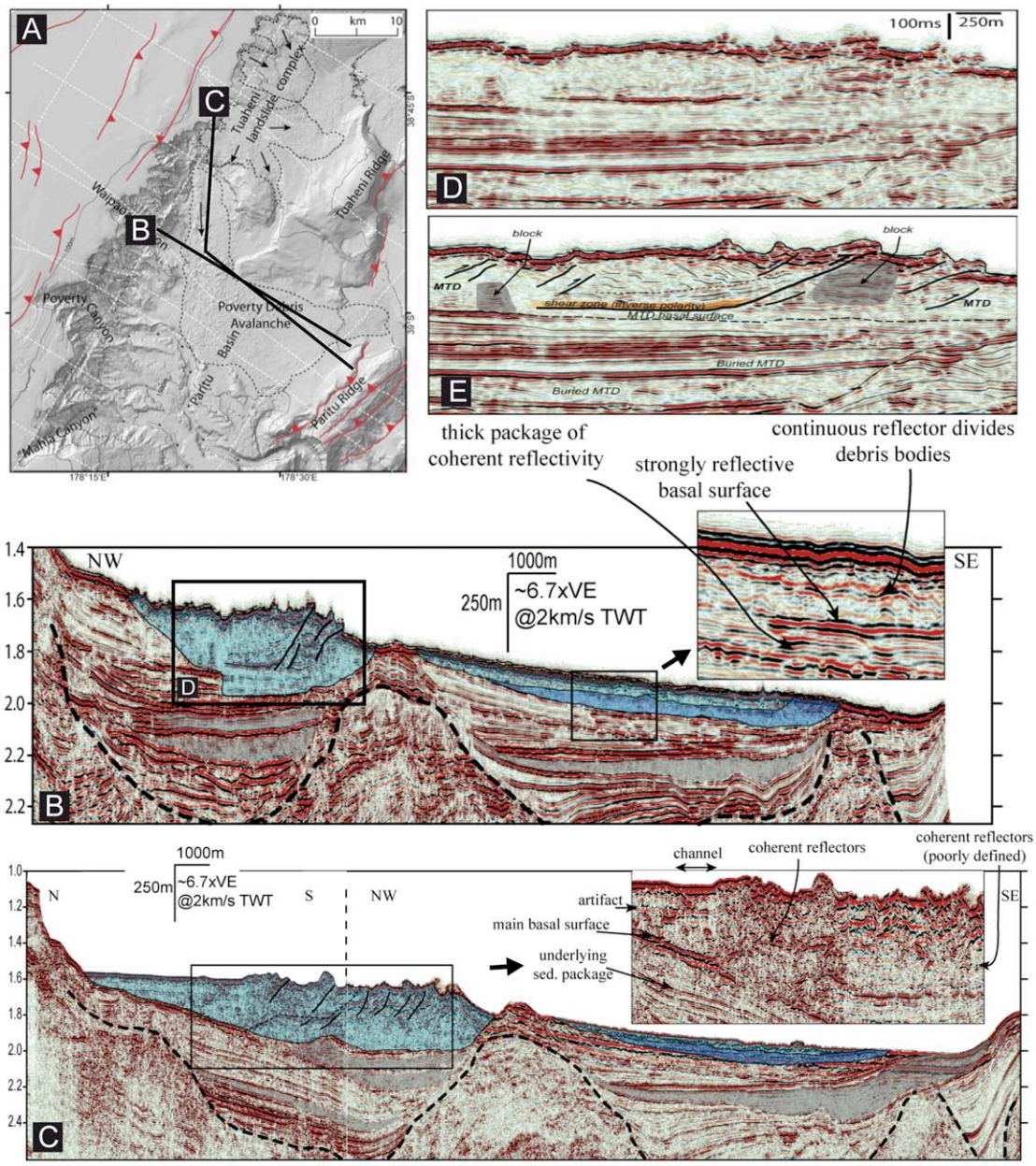

914

915 Figure 9: A) Shaded relief map showing the location of the following MCS profiles
916 (B, C and D), extent of the landslide deposits (dotted line) and the interpreted
917 source area. Inferred directions of transport (black arrows) and main thrust
918 fault traces (red toothed lines). B) MCS profile of the Poverty MTC (light and
919 dark blue overlays represent the two main component bodies) showing its
920 internal reflections and the host stratigraphy characterized by buried MTDs
921 (gray overlay). In the inset is represented an enlargement of the MCS profile
922 in the distal part of the MTC, showing the amalgamation between at least two

MTDs (weak continuous reflector) and the basal shear zone (strong discontinuous reflector). C) MCS profile of the Poverty MTC roughly parallel to the line represented in B with inclusion of the most proximal zone and part of the headwall slide scar. The same features observed in B are labeled. The inset represents a close-up of the MCS profile in the proximal part of the MTC characterized by the thickest accumulation and overall compressional regime, as testified by the dominance of thrust faults. D) Slice and E) interpretation of part of the MCS profile of B with indication of the main recognizable features. Note the structurally confined depositional patterns of the sedimentary cover. The weak, discontinuous reflectors characterizing the slide blocks and the strong, coherent reflector representing the main basal shear zone and the flat part of a ramping thrust fault cutting the entire deposit. Modified from Mountjoy and Micallef (2012).

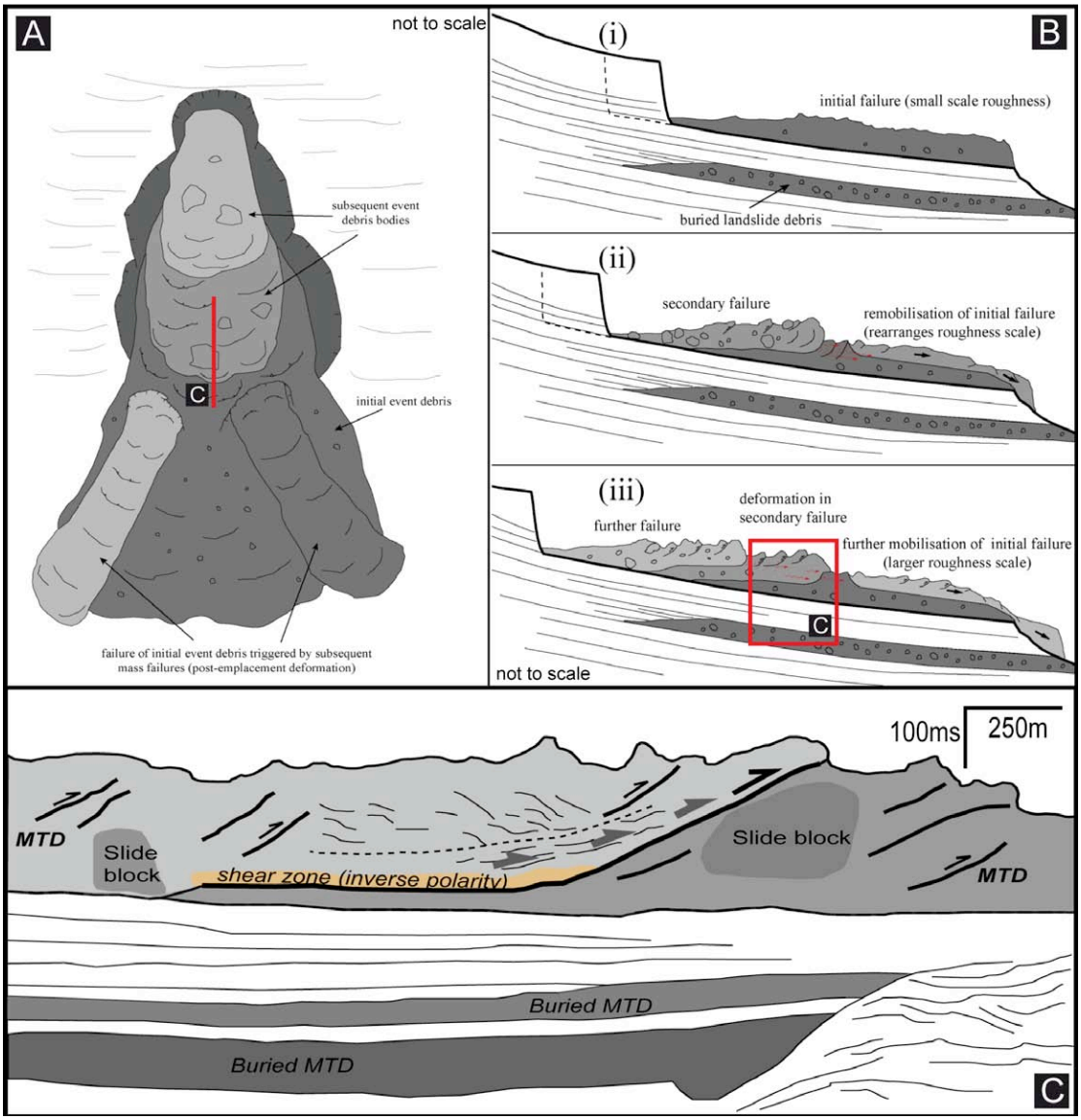

936

937 Figure 10: A) Schematic cartoon showing the morphology and the main superficial
938 features of the Poverty MTC in plan view. B) Conceptual scheme showing the
939 three evolutionary stages (from i to iii) of the inferred retrogressive landsliding
940 process, the slide masses' amalgamation and the consequent re-destabilization
941 of the upper, frontal part of the preceding deposit (i.e. "progressive
942 landsliding"). C) Simplified representation of the MCS profile slide of fig. 9D
943 and 9E with identification and interpretation of the main actual structures. To
944 insert the interpreted profile in the proposed framework, the approximate
945 position of the synthetic profile slice has been labeled in A and B.

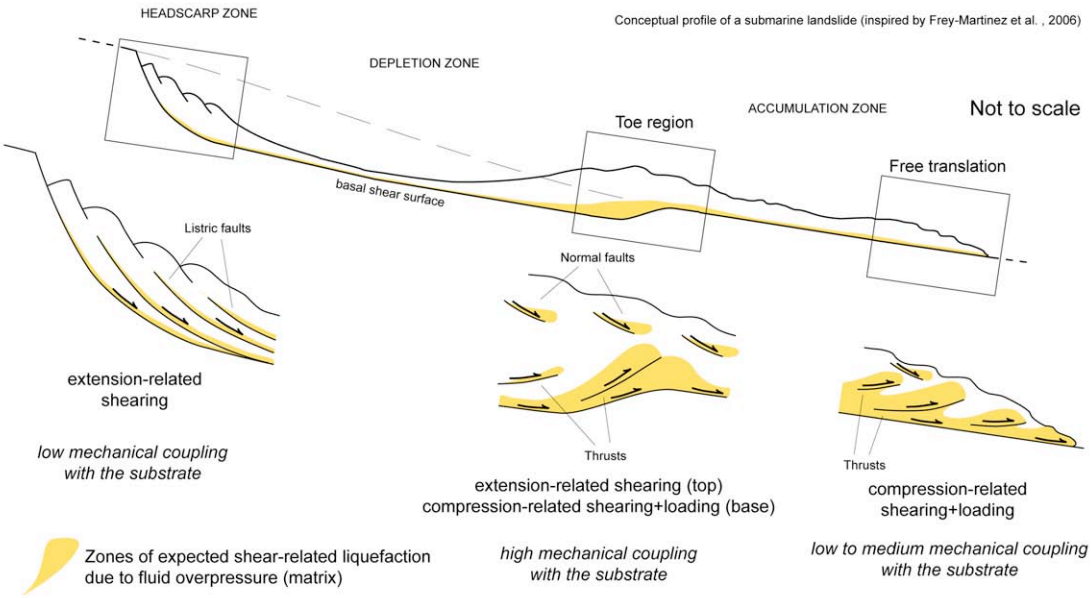

946

947 Figure 11: Conceptual profile of a submarine landslide complex with identification of
948 the possible zones where the bulk of mass transport-related deformation
949 occurs and indication of the inferred deformation mechanisms. Relatively
950 thick, matrix-dominated portions and matrix-rich shear zones are thought to
951 represent the products of such localized enhanced progressive deformation
952 (from extensional to compressional, and combination thereof), characterizing
953 specific portions of the MTD which in turn roughly define the three main steps
954 of the slide evolution. Inspired from Frey-Martinez et al. (2006).

955